

Sensitivity Analysis and Optimization of Delta Wing Design Parameters using CFD-Based Response Surface Method

M. Aelaei[†], S. Karimian and F. Ommi

Department of Mechanical Engineering, Tarbiat Modares University, Tehran, P.O.B. 14115-111, Iran

[†]Corresponding author E-mail: mohammad.aelaei@modares.ac.ir

(Received October 9, 2018; accepted January 30, 2019)

ABSTRACT

This paper explores the effect of design variables on the objective functions of clipped delta wing with a modified double-wedge airfoil section based on parametric analysis and CFD-based optimization using response surface method. This type of wing is used in air-launch-to-orbit vehicles. The thickness, wing-span, tip chord, leading edge radius, front diagonal edge and rear diagonal edge lengths are defined as design variables and aerodynamic efficiency, drag and lift coefficients as objective functions. The analysis was performed at Mach 0.85 and 1.2 and for several angle of attack (AOA). The optimization process is performed by numerical stimulation of the flow around the wing at different Mach numbers and AOAs for the deformed geometry at each step including 368 cases. Minimizing the drag force and maximizing both lift coefficient and aerodynamic efficiency have been selected as optimization goal. The evolutionary optimization technique of NSGA-II (Non-dominated Sorted Genetic Algorithm-II) in combination with the RSM has been used, which leads to distinct but very close candidates for each flight conditions. Defining the critical design point, it can be deduced the aerodynamic efficiency will be increased by 50% compared with base wing model. Finally, it is shown that the best point for optimizing the air-launched vehicle equipped with delta wing in the ascent trajectory, is the maximum angle of attack that occurs at Mach 1.2.

Keywords: Delta wing; Air launch-to-orbit vehicle, aerodynamic efficiency; NSGA-II Optimization; Response Surface Methodology.

NOMENCLATURE

$a = \sqrt{\gamma RT}$	speed of sound	R	universal gas constant or correlation matrix
AR	Aspect Ratio	S_{ref}	reference area
A_i	lagrange multipliers	T	temperature
A_i^*	lagrange multipliers	T_0	total temperature
C_D	drag coefficient	TR	Taper Ratio
C_L	lift coefficient	W	weight and weighting vector
C_{Lmax}	max lift coefficient	$W_{pegasus}$	pegasus weight
C_t	tip chord	W_{model}	model weight
C_r	root chord	x_i	N-dimensional vector
D	drag force	α	angle of attack
I	unit tensor	ρ	density
L	lift force	ρg	gravitational body force
$l(\xi)$	generic loss functions	μ	molecular viscosity
M	Number of Design Variables	$\gamma = \left(\frac{c_p}{c_v}\right)$	ratio of specific heats
$M = u/a$	Mach Number	τ	stress tensor
M_w	molecular weight		
N	sample data Points		
P	static pressure		
P_0	total pressure		
P_{OP}	operating pressure		

1. INTRODUCTION

The Delta Wing is the first choice for the initial design and optimization of the high AOA aerial vehicles. The delta wing is one of the most commonly choice for aircrafts and missiles, which is used in the Pegasus air launch-to-orbit rocket (Mendenhall, 1994). The first reason for using delta wing is the maneuverability of this wing. The delta wing stalls at higher angle of attack than the conventional wings. Some other reasons for using the delta wings include: better aerodynamic performance in high speed, reduced loading on the wing area unit due to the larger surface area compared with the conventional wings, the use of a more robust structure and extensive root installation on the body, and the inherent observance of the area's law in design (Anderson Jr, 2010). A delta wing is called slender with a leading-edge sweep angle larger than 60° and called Non-slender with a sweep angle smaller than 60° (Verhaagen & Elsayed, 2008). Although reference (Gursul, Gordnier, & Visbal, 2005) defines a non-slender wing as having a leading-edge sweep equal to or less than 55° . The behavior of the slender and non-slender delta wings has distinct differences (Gursul, Gordnier, & Visbal, 2005). In order to achieve the high maneuverability of advanced aircrafts, it is necessary to understand the starting and generation of vortices, their collapse and control (Nangia, 2008). The flow over a delta wings with sweep angles greater than 45° is governed by two counter-rotating vortices evolved from the leading edges. At moderate to high angles of attack, two dividing streamlines are formed on lower surface of the wing, similar to the forward stagnation point in 2-D flow. Flow inboard of this dividing streamline just travels downstream, swept along by streamwise component of velocity. The outboard flow in vicinity of the leading ledge travels out and tries to curl around the leading edge to upper surface (Görtz, 2005). After separating from the leading edge, the free stream turns into curved free shear layers on delta wing surface (Gursul, Zhijin, & Elen, 2007). A delta wing creates a characteristic vortex pattern over the upper surface which enhances lift force. As the angle of attack increases, the leading edge of the wing generates a vortex that energizes the flow on the upper surface of the wing, delaying the flow separation, and giving the delta a very high stall angle.

The results of the researchers show that the tip vortices are a function of the AOA, Mach and the Reynolds number, while the change in position and length of these vortices depends on the leading edge radius, AOA, and the Reynolds number (Nangia, 2008) (Breitsamter, 2008). Although ref (Roos & Kegelman, 1990) showed that in addition to the above, flow behavior depends on the wing sweep angle. The vortex flow structure is fundamentally different on a non-slender with sharp edges with slender delta wing (Taylor, Schnorbus, & Gursul, 2003). The flow on the non-slender delta wings has highly unsteady (Gursul, Gordnier, & Visbal, 2005). Non-slender delta wings are more sensitive to AOA variations than slender delta wings (Verhaagen &

Elsayed, 2008). Reference (Mendenhall, 1983) explains the application of delta wings on the aircraft comprehensively. Reference (Polhamus, 1968) provides an analytical method for estimating the force coefficients in a delta wing with assumption of potential flow. Most of the analytical methods have been applied in the form of corrections for leading edge shape and Mach numbers. (Bertin & Smith, 1998) Among the extensive literature that investigated the delta wing with numerical methods, reference (Morton, Forsythe, Mitchell, & Hajek, 2002) simulates the fluid flow on a delta wing using RANS and DES methods and reference (Mitchell & Ramesh, 2016) with Euler and RANS methods in the ANSYS-Fluent has been reviewed and then optimized the wing with the goal of minimizing pressure distribution. Reference (Gursul, 2005) has reviewed the numerical methods for simulation of flow on a delta wing. In references (Bertelrud, *et al.*, 2000) and (Malik, Fei, & Meelan, 2007) experimental and numerical data are presented on the transient flow on the Pegasus wing. Reference (Noffz, 1991) has examined the heating and thermal protection of the Pegasus wing and ref (Godil & Bertelrud, 1992) describes the Pegasus wing glove design for a hypersonic cross-flow transition and discusses sensitivity of variation of wing thickness, leading edge radius, trajectory variations and surface temperature.

The lift force required to reach the target orbit is estimated from the trajectory analysis. To meet the lift requirement, a necessary CL value needs to be calculated (Jacob, Bret, & Peter, 2016). In the design of a winged air launch-to-orbit rocket, the most important conditions in the ascent trajectory are the initial condition of the rocket (1st stage ignition), the highest angle of attack, and the maximum dynamic pressure condition, so the wing should be evaluated for this scenario. It may be also suitable for design and optimization of the wing. The evaluation and optimization carried out in this research will give insight for selection of critical point. The first stage ignition (starting condition) occurs at an altitude of 12 km and $M=0.85$ with $AOA=14^\circ$ and the highest angle of attack occurs at an altitude of 12 km and $M=1.2$ with $AOA=20^\circ$. Also, the maximum dynamic pressure condition is close to this latter situation. Therefore, these two situations are selected for parametric analysis. For this purpose, we consider a cropped delta platform with a modified double wedge airfoil section (Mendenhall, 1994) like the Pegasus wing. Rather than the leading edge radius that is curved, the rest of the plates are flat.

In the current research, 368 objective sample points were solved by employing the Navier–Stokes equations and applying the Unsteady Reynolds averaging method (URANS), by employing the $k-\omega$ SST turbulence model and using hybrid mesh. The diagrams of the main factors were examined to find out which design variable affects the objective function.

2. WING DESIGN AND GRID GENERATION

The process for designing the wing will be done by

Table 1 Lift coefficient variation and grid independence study

Number of cells (millions)	Lift coefficient at M=1.2, flight condition	% Error relative to the densest mesh response
0.62	0.993	5%
0.97	0.978	0.4%
1.59	0.984	0.2%
3.81	0.982	0%

varying the shape of the wing by changing the design variables (input parameters) in order to maximize lift force and minimize drag force (output parameters) in such a way as to increase the aerodynamic efficiency. In such situation, the model wing will be optimized for minimum drag with an equality constraint for lift at flight condition. The first step of any design simulation is to create the model, this step is also used to define the input parameters (Design Variables) to be investigated (*Design Xplorer User's Guide, 2016*). In this design, the sweep angle is considered constant (45°), which is classified in the non-layered delta wings. The thickness, wingspan, tip chord, leading edge radius, front diagonal edge and rear diagonal edge lengths are defined as design variables. The wing configuration and airfoil section with design variables have been shown in Fig.1. According to the delta wing concept, the root chord of the wing is a dependent variable which varies with tip chord and span variation. It is shown in Fig. 2. that the wing is mounted on the air launching vehicle body.

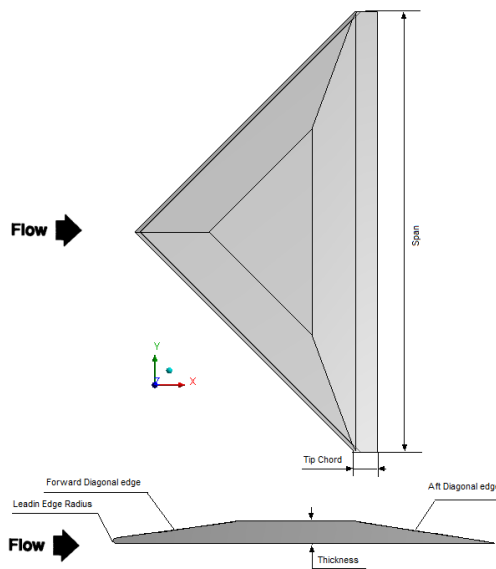


Fig. 1. Wing configuration and airfoil section with design variables used in the analysis.

The domain of the flow around the wing is created in such a way that due to the parabolic equations in high Mach numbers, the boundary condition error in the numerical solution can be neglected. After this, the tetrahedron mesh with 971,000 cells in the parabola computational domain were generated. (Fig. 21) The inflation grid with 16 layers of hexahedral mesh

around the wing for accurate simulation in the vicinity and the rest with tetrahedron are structured and extended around 25 chords upstream, 40 downstream and 20 on the side.

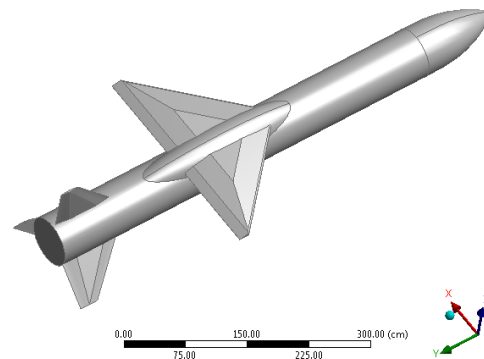


Fig. 2. Wing mounted on the Air launch-to-orbit vehicle.

In the simulation of the viscous flow with the RANS equations, due to the existence of a normal velocity gradient on the wall near the wing surface (boundary layer), one of the effective parameters in convergence and proper mesh quality is the orthogonality. In order to meet this requirement, the tetrahedron mesh with minimum orthogonality quality 0.12 is achieved in mesh generation. To verify the independence of the mesh, the number of grids has been tested from 618 thousand cells to 3.81 million cells. In the Table 1 lift coefficient variation with the number of mesh and the relative error to the finest mesh response has been shown. The Y^+ measurement in all tested meshes of this calculation is in the range of $30 < Y^+ < 300$, which means using the wall function in the first cell. The density of cells around the rocket, due to the larger flow gradients in this area, is significantly higher than the farfield in the solution domain.

To confirm the results for the present study, comparisons of numerical and Pegasus rocket experimental data to Pegasus XL (*Ridolfi, Pontani, & Teofilatto, 2010*) were done and the results are shown in Fig. 3. where the lift coefficient is a good quantitative agreement.

3. NUMERICAL METHOD

The numerical calculations were performed by solving the 3D Navier-Stokes and energy equations using finite volume based CFD software Ansys Fluent at $M=0.85$ and 1.2 , $AOA=0, 5, 14$ and 20° and

with physical properties values dictated by the flight condition at ascent to orbit trajectory. The angle of attack of the wing has a major impact on the aerodynamic properties, AOA=14° at M=0.85 is the first stage ignition condition, and AOA=20° at M=1.2 is the maximum angle of attack in the ascent trajectory. The Unsteady Reynolds Average Navier-Stokes (URANS) approach analysis was performed using the κ - ω SST model which has been shown to give relatively accurate predictions in fluid flow analysis (Bardina, Huang, & Coakley, 1997). Shear Stress Transport κ - ω turbulence model can predict the flow separation process with higher accuracy. A key advantage of RANS method is the decline in computational resources, which has made it a common choice of adoption in practical industrial applications (Younis, Bibi, Haque, & Khushnood, 2009). The k - ω model based on RANS uses the Boussinesq hypothesis for computing turbulent viscosity (Younis, Bibi, Haque, & Khushnood, 2009). Second order upwind discretization scheme is applied for momentum, κ and ω . No-slip wall conditions are applied to the wing surfaces without any roughness. Due to the compressibility of the flow, the type of solver is set to density-base. The density-based solver uses the continuity, momentum, energy, and species equation simultaneously to linearize the governing equations to create a system of equations for the dependent variables. Other settings have been shown in Table 2. The convergence of the steady state situation is reached when the residuals are reduced by the ratio of less than 1e-03 and the lift coefficient is fixed in more than 200 iterations within 0.01% error. The reference area of the wing is 2.16 m² and the reference length is 1.476 m.

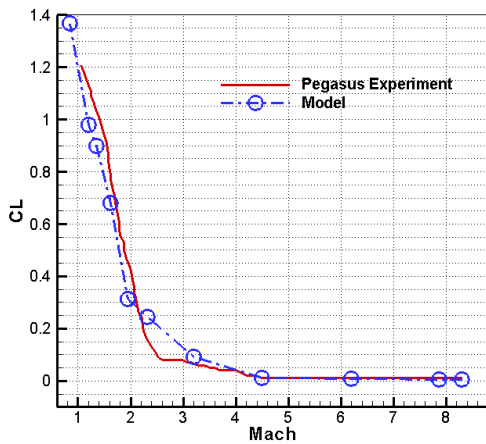


Fig. 3. Comparison between Experimental and Numerical data.

Compressibility of flow is characterized by the value of Mach number. The objective functions of optimization process are defined as Eqs. (1) and (2). (Anderson, 2003).

$$L = \frac{1}{2} C_L \cdot \rho \cdot A \cdot u^2 \quad (1)$$

$$D = \frac{1}{2} C_D \cdot \rho \cdot A \cdot u^2 \quad (2)$$

Where L and D are the lift and drag forces, C_L and C_D are the lift and drag coefficients, ρ is air density A is reference area and u is the flow velocity.

Table 2 Settings of CFD Simulation

Parameter	Type/quantity
Fluid Type	Air
Solver	steady, 3D, density-based
Formulation	implicit
Flux type	Roe-FDS
Discretization method	2nd Order Upwind
Boundary condition	Pressure Farfield-Wall
Turbulence model	$k - \omega$ SST
Courant number	0.5>
Reference pressure (pa)	0
Operating pressure (pa)	16510.4
Temperature(°C)	216.65
Velocity (m/s)	353.95
Density (kg/m ³)	0.2564972

4. ANALYSIS PROCEDURE

4.1 Design of Experiment

The main purpose of design exploration is to identify the relationship between the performance of the product and the design variables. DoE and response surfaces provide all of the information required to achieve Simulation Driven Product Development. DoE is a technique that assists in the numerical analysis of performance parameters or in determining an efficient experimental process (Design Xplorer User's Guide, 2016). A DoE method determines how many and which design points should be solved. This method generates the points but does not solve them or generate and solve a DoE Design Point matrix (Hyun-Su & Youn-Jea, 2016). This method can provide an appropriate output chart that can be used by researchers to determine the optimal point among several parameters. This technique is also capable of analyzing the interactions of each industrial process and presents the relationship between the inputs and outputs of each process in the form of a statistical model (Manshadi & Jamalinasab, 2017). To evaluate the aerodynamic efficiency (L/D) according to the change in design variables of wing, 46 CFD-based flow analyses at each AOA and Mach number were conducted using orthogonal array in the context of DoE, a total of 368 evaluation. The DoE table is first filled in by the sampling values in the design space. Each design parameter can be combined with others at different levels. The DoE table is generated using the optimization software DX by ANSYS.

4.2 Response Surface Methodology

The Response Surface Methodology (RSM) is a graphical representation that allows you to see how changes to each input parameter affects a selected output parameter, and the relationship between different variables and responses (Adeeb, Maqsood, Musthaq, & Sohn, 2016). This process is much

Table 3 Initial design parameters and constraint values

Quantity (cm)	Base Value	Lower limit	Upper limit
wing semi-span	134.12	110.71	147.53
Tip Chord	13.52	11.17	14.87
Thickness	8.12	6.31	8.93
Leading Edge Radius	2.5	2	2.75
Front diagonal edge length	31.76	28.58	34.94
Rear diagonal edge length	40	36	44

quicker to use than direct searches of the CFD (Design Xplorer User's Guide, 2016). SRM is the sequential heuristic that no attempt to solve the flow conditions over the wing configurations being selected. The response surface methodology, especially the central composite design (CCD) method, which is used in this research, is a technique in which orthogonal arrays are used to investigate a large number of design parameters.

By specifying the design type of CCD, it is possible to improve the response surface fit for DOE studies. For each CCD type, the alpha value is defined as the sampling point location that accounts for all quadratic main effects (Design Xplorer User's Guide, 2016). In this study, a Face-centered type of CCD has been used which is a three-level design with no rotatability with the alpha value equals 1.0.

Central Composite Design combines one center point, points along the axis of the input parameters, and the points determined by a fractional factorial design (Kleijnen, 2015) (Design Xplorer User's Guide, 2016). The use of the CCD method allows the second order response to be matched for each performance characteristic of the analysis with various techniques, including multivariate regression, and the data obtained from the response surface for the rapid evaluation of the independent variables in combination and using the optimal Non-linear optimizer to be used (Engelund, Stanley, Lepsch, McMillin, & Unal, 1993). A total of 46 numerical solutions in each Mach number and AOA were found to be sufficient to calculate the coefficients of the second-order polynomial regression model for 6 variables and the effects of each of these parameters on the lift and drag forces and aerodynamic performance were studied. The initial design parameters and constraint values for the CCD type of the DOE matrix are shown in Table 3.

The Non-parametric Regression method has been used to create the Response surface. This method uses Support Vector Regression. It is similar to Kriging in that the prediction depends on current data. But instead of using all data, this method chooses the most important data points to perform prediction. Thus its computation cost for prediction is less than that of Kriging. Yet, its cost of fitting is still high. The model does not fit through the data. (Design Xplorer User's Guide, 2016). This is convenient method when the data is highly nonlinear, and the model is fitted right through the important data. Goodness of fit which evaluates the accuracy of response surface is shown in Fig. 4. At the Non-parametric Regression, if the input sample

(as generated from a DoE method) is $= \{x_1, x_2, x_3, \dots, x_M\}$, where each x_i is an N-dimensional vector and represents an input variable. More details of RSM are given at Design Xplorer User's Guide, 2016

Goodness fit data is used to inform for any of the output parameters in a response surface. If any of the input parameters is discrete, a different response surface is built for each combination of the discrete levels and the quality of the response surface might be different from one configuration to another (Design Xplorer User's Guide, 2016). Goodness of Fit is closely related to the response surface algorithm used to generate the response surface (Barret, 1996) Goodness of fit which evaluates the accuracy of RS is shown in Fig. 4.

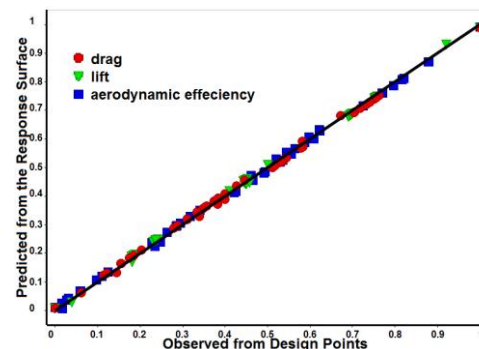


Fig. 4. Goodness of fit for evaluating the accuracy of response surface.

To find out how sensitive the optimized results are in terms of small changes in design inputs derived from the proposed model, RS analysis has been performed and the obtained results are shown in Figs. 7 to 18.

By examining the RS in $M=0.85$, it was observed that with by increasing the thickness, the drag coefficient increases gradually at 0° and 5° angle of attack, with the difference that the gradient increases by 5 degrees, but at AOA of 14° and 20° decreases. Increased thickness means higher profile drag in subsonic flight regime and higher wave drag in transonic and supersonic flight regime (Roskam, 2002). The lift coefficient at $AOA=20^\circ$ approximately is constant, but decreases in other angle of attacks. This response to thickness change, increases the aerodynamic performance at $AOA=20^\circ$ but at the rest angle of attacks is constant which shown in Fig. 5. In a supersonic flight regime, the wave drag is proportional to the parameter $(t/c)^2$, because of very rapid increase of wave drag with t/c ,

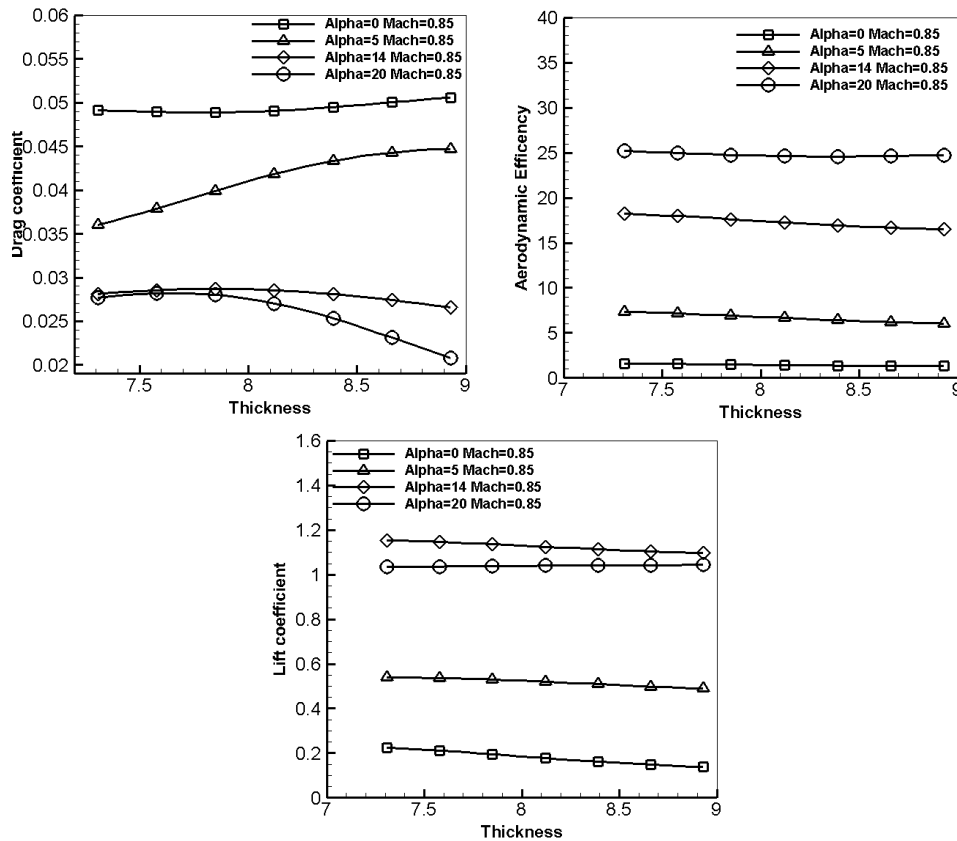


Fig. 5. Effect of increasing thickness on the objective functions at $M=0.85$ and $AOA=0, 5, 14$ and 20° .

therefore, the thickness of wing must be selected very carefully (Roskam, 2002). The reference (Gülsaçan, Şencan, & Yavuz, 2018) has shown that the effect of t/c on the flow structure is significant, such that, as the wing thickness increases, the flow structure is transformed from the leading edge vortex to the three-dimensional separated flow regime. Also, the lowest t/c ratio wing might be more resistive to the stall conditions.

Increasing the leading edge radius increases the drag coefficient at all angle of attacks except the zero angle, but does not affect the lift coefficient so much. Aerodynamic efficiency drops as the leading edge radius increases at high AOAs. At low speeds, increasing the L.E. radius are beneficial in producing the large value of $C_{L_{max}}$ (Roskam, 2002). Due to the greater impact of the drag force by increasing the LE radius, the aerodynamic efficiency reduces at higher angle of attacks, but at the lower angles, the impact is very small and reduces aerodynamic efficiency. This behavior is due to the fact that the size and strength of the primary vortex tend to be weakened by increasing the L. E. radius. Reference (Elsayed, Scarano, & Verhaagen, 2008) has investigated the effects of different leading edge shapes, which shows that a more rounded leading edge narrows the primary-vortex footprint and moves the vortex burst closer to the trailing edge. Also, the more rounded leading edge actually generates smaller vortices and moreover tends to increase the magnitude of the

vorticity in the first part of the free shear layer. This process is presented in Fig. 7.

Wing Span is one of the entrances that has a great impact on the increase of both lift and drag coefficients at high subsonic regimes. At low AOAs, the effect of this increase on the lift coefficient is greater than on the drag, which is also observed in the aerodynamic performance of the wing. As the angle of attack increases, the drag coefficient increases more than the lift coefficient, therefore the aerodynamic efficiency decreases, but at the $AOA=14$, this trend becomes a significant change so that aerodynamic efficiency is first reduced and then increased. Figure 8 shows this trend. Increasing the wing span is obtained by increasing the wing size and aspect ratio ($AR=b^2/S$). Also, increasing the wing size causes the lower wing loading and vice versa. The wing size decrement also will attenuate the total weight which is by itself one of the important goals in optimizing the air-launching vehicle. High AR wing tends to have high lift curve slope, lower induced drag (drag due to lift) and therefore larger values of $(L/D)_{max}$. Although high AR wings create less induced drag, they have greater parasitic drag, (drag due to shape, frontal area, and surface friction), so the drag and lift forces are increased.

The effect of increasing the tip chord at $M=0.85$ on the drag coefficient at zero angle of attack is significant and the drag force accordingly decreases,

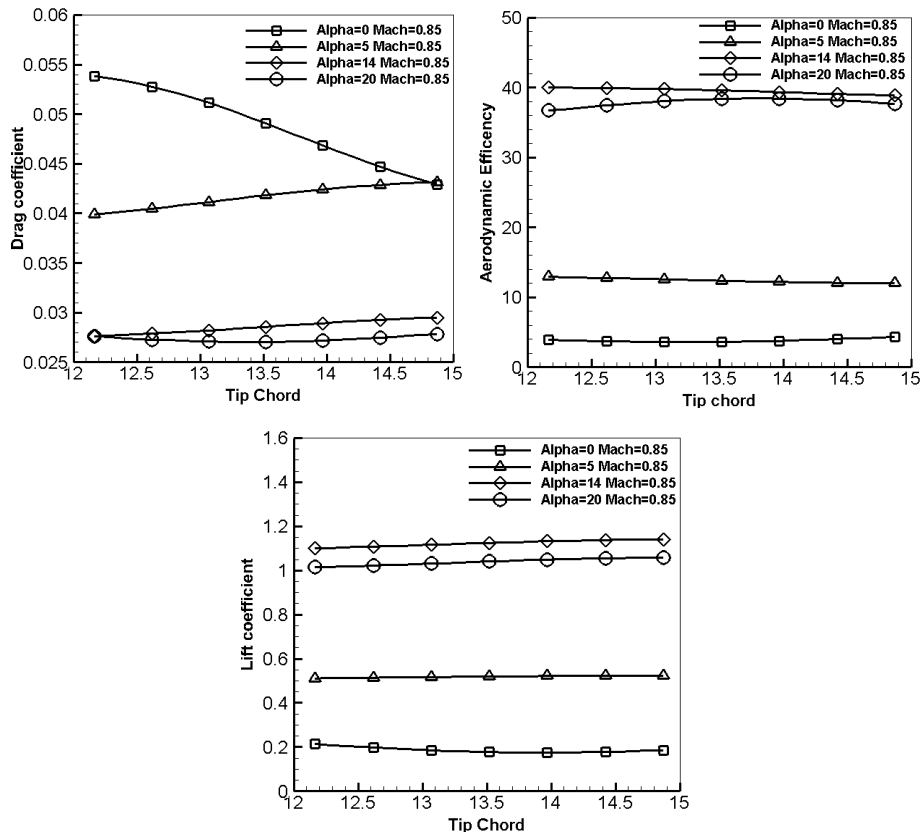


Fig. 6. Effect of increasing tip chord on the objective functions at $M=0.85$ and $AOA=0, 5, 14$ and 20° .

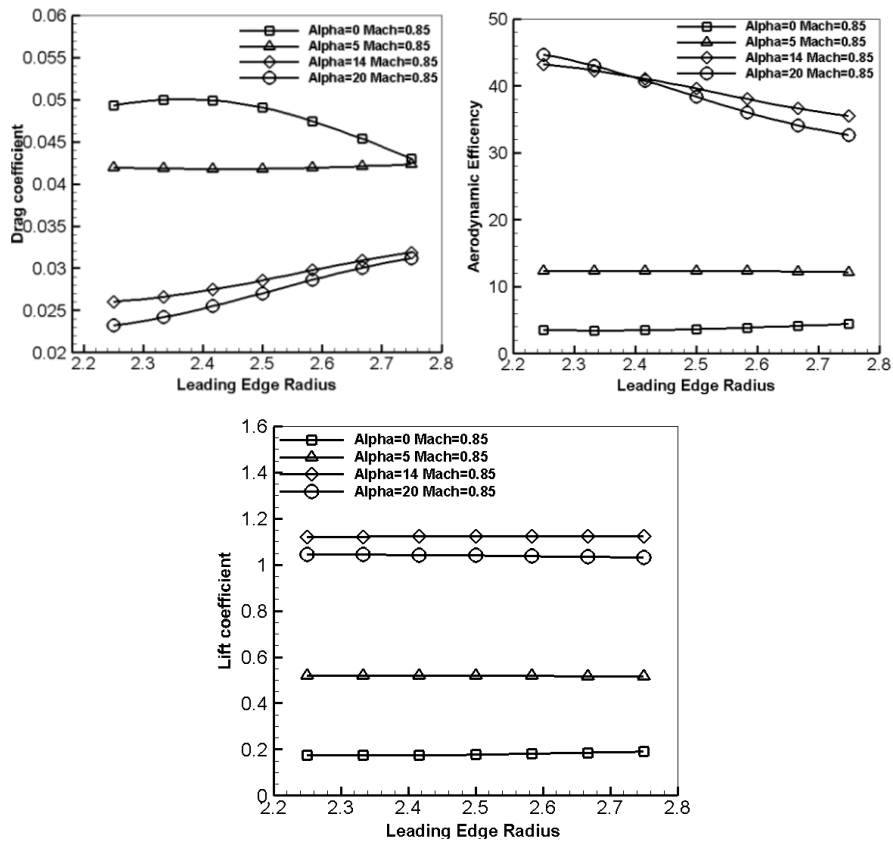


Fig. 7. Effect of increasing leading edge radius on the objective functions at $M=0.85$ and $AOA=0, 5, 14$ and 20° .

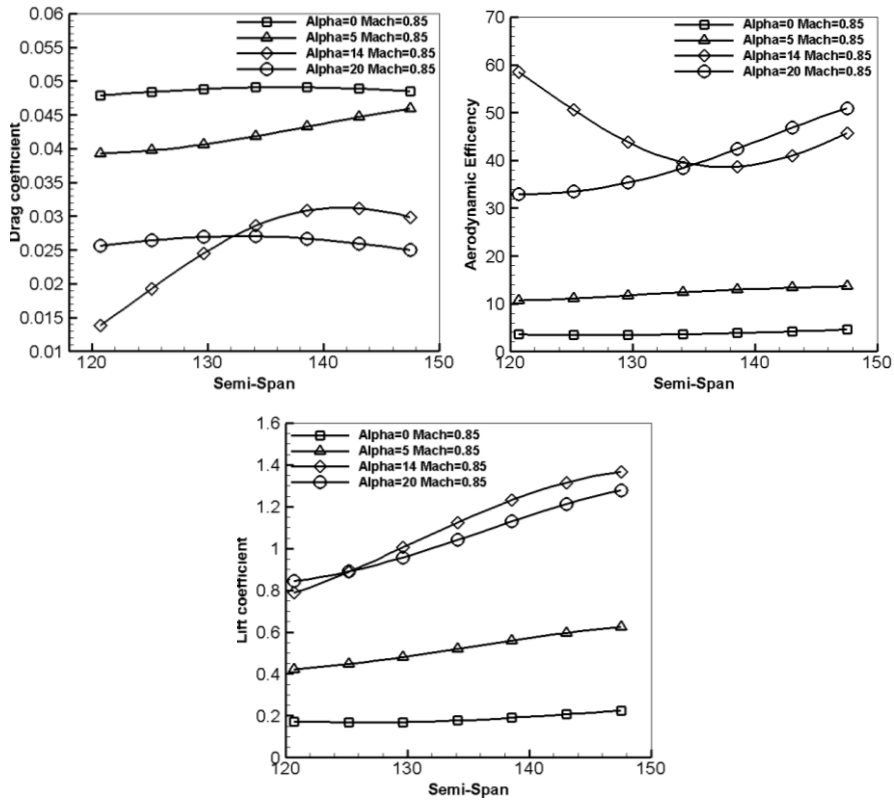


Fig. 8. Effect of increasing span on the objective functions at $M=0.85$ and $AOA=0, 5, 14$ and 20° .

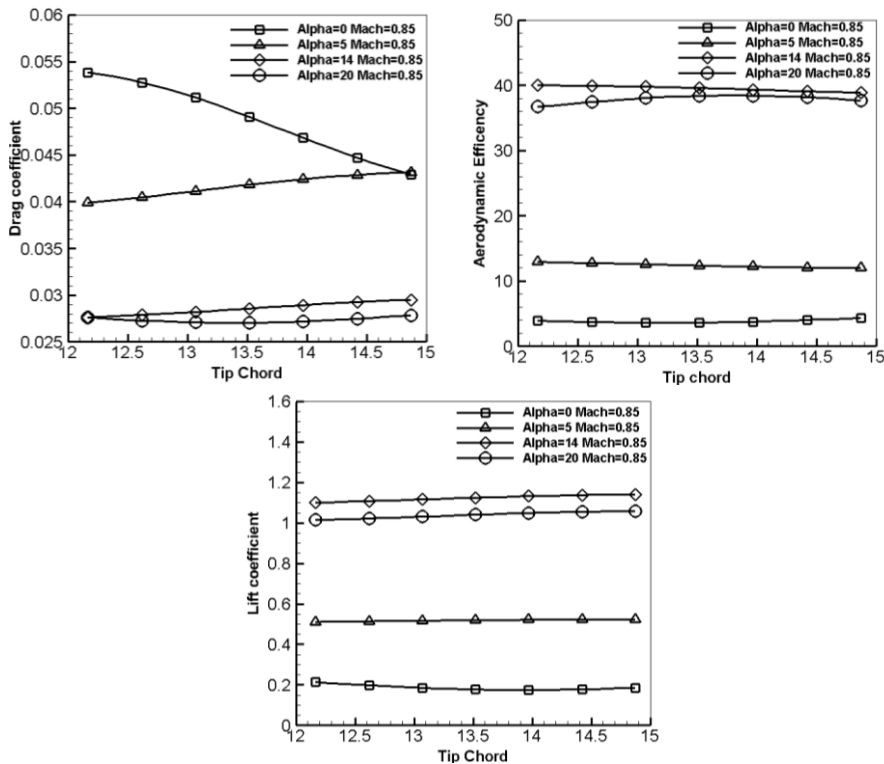


Figure 9, The effect of increasing tip chord on the objective functions at $M=0.85$ and $AOA=0, 5, 14$ and 20°

but with increasing the AOA, the drag coefficient increases slightly. This trend can also be seen at lift coefficient, and has a positive effect on the lift force at all AOA except zero angle. In total, the increase

in the wing tip chord has improved the aerodynamic efficiency at zero AOA, but has a negative effect by increasing the angle of attack as shown in Fig. 6. Increasing the tip chord increases the taper ratio

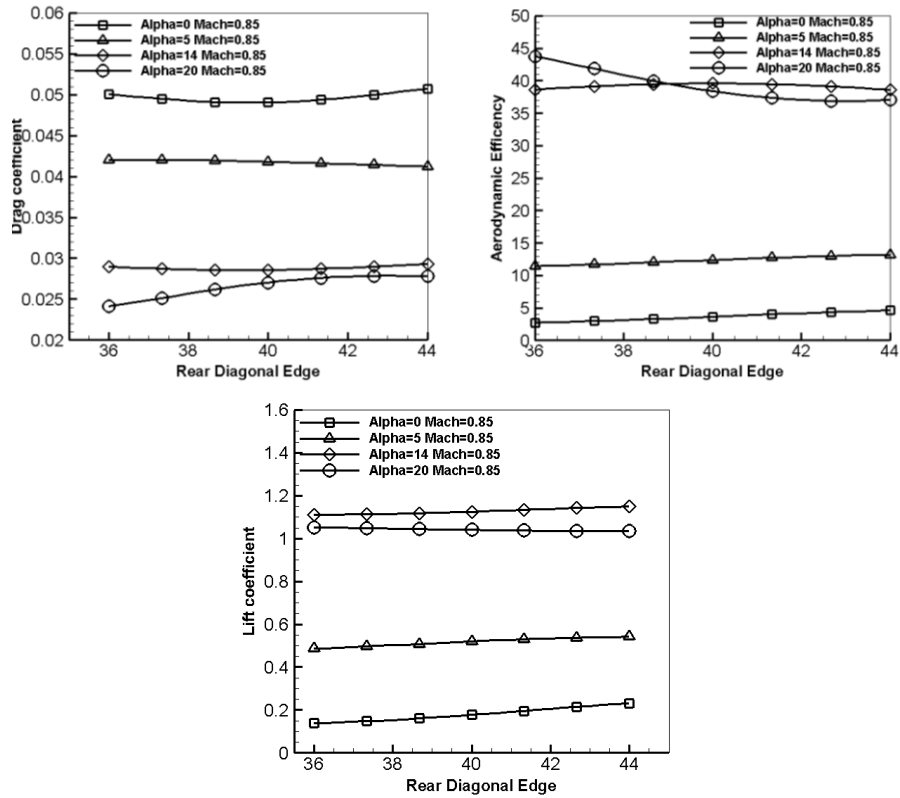


Fig. 10. Effect of increasing rear diagonal edge length on the objective functions at $M=0.85$ and $AOA=0, 5, 14$ and 20° .

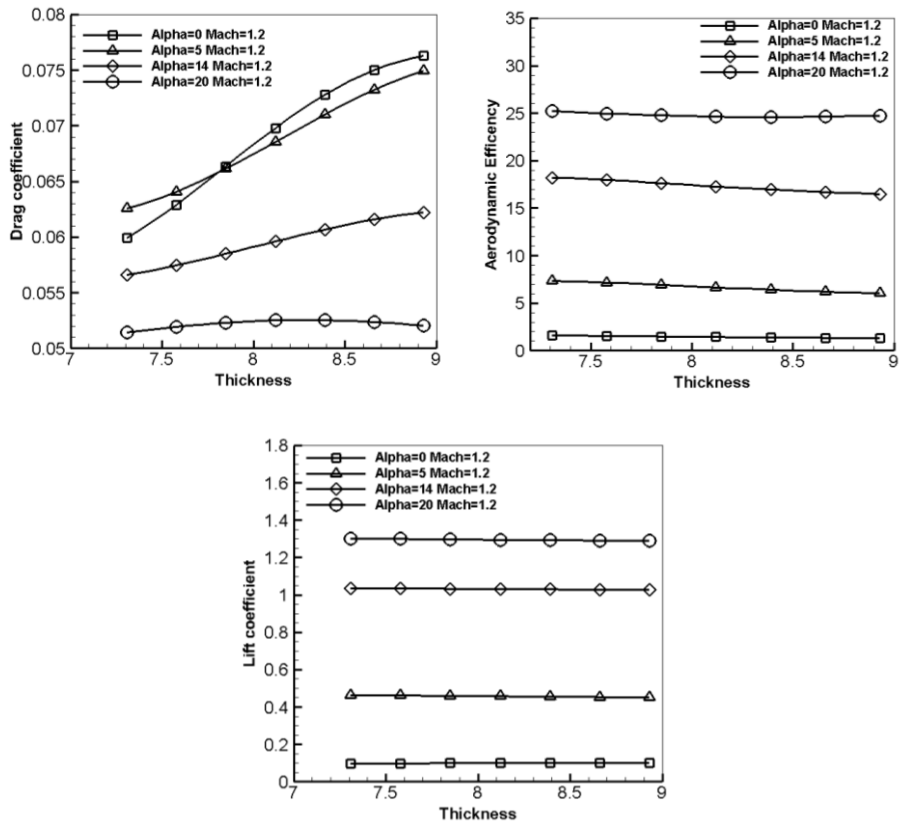


Fig. 11. Effect of increasing thickness on the objective functions at $M=1.2$ and $AOA=0, 5, 14$ and 20° .

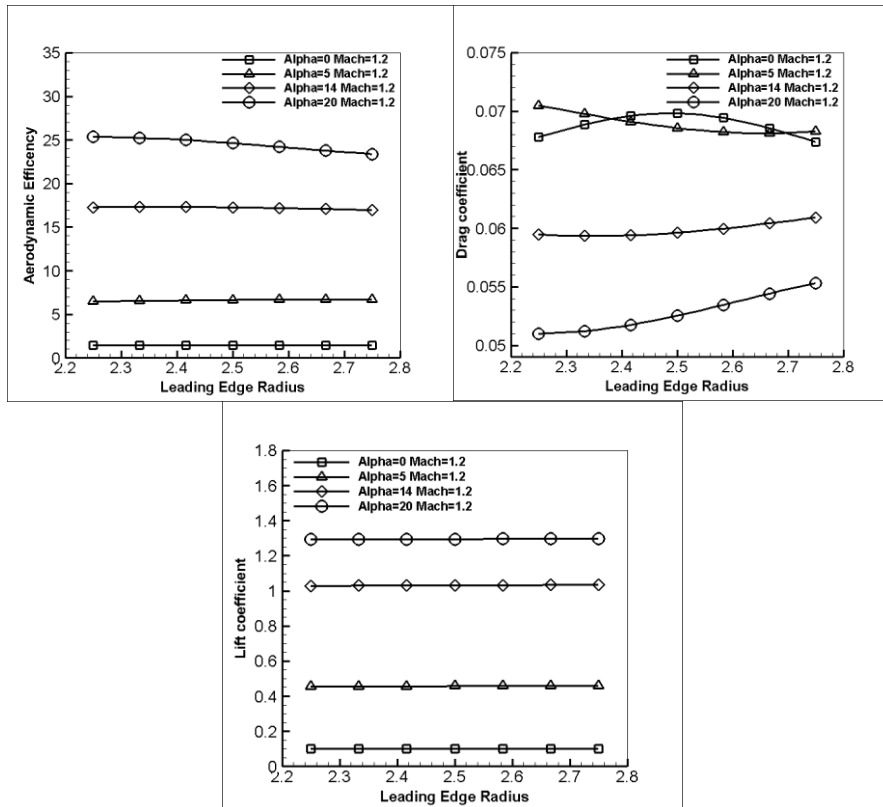


Fig. 12. Effect of increasing leading edge radius on the objective functions at M=1.2 and AOA=0, 5, 14 and 20°.

($TR=C_l/C_d$), in addition, it also affects the wing size, weight and tip stall. Increasing the lift and drag forces is due to the fact that the tip vortices affects a large portion of the upper wing surface and the low pressure area caused by the vortices. The tip vortex causes downwash, which decreases the effective angle of attack at high angles and it will lead to increase the drag force. The tip vortex forms a low-pressure region on the upper surface of the wing, which provides additional lift force (Lian, Wei, Dragos, & Baoning, 2003).

The effect of front diagonal edge length at M=0.85 on the lift and drag coefficients is very low. Of course, at zero AOA, both lift and drag coefficients increase, but due to the greater impact on the lift, the aerodynamic efficiency improves. However, the increase in front diagonal edge length of the wing at high AOA, has a negative effect on the drag force and has increased. Also, as the front diagonal edge length increases, the lift coefficient increases at low AOA slightly. Altogether, this trend is reflected in the aerodynamic efficiency, so that it improves at low AOA and decreases with the increasing angle of attack, as shown in Fig.9. This behavior is due to the relative reduction of the slope of the front diagonal edge length.

The effect of rear diagonal edge length variation on the lift and drag coefficients is like front diagonal edge length. This impact on the lift force has been quite positive. At zero AOA, both lift and drag coefficients increase, but due to the greater impact on the lift, the

aerodynamic efficiency improves. The increase in rear diagonal edge length of the wing at high AOA, has a negative effect on the drag force and has increased. Also, as the rear diagonal edge length increases, the lift coefficient increases at low AOA slightly. The aerodynamic efficiency improves at low AOA and decreases with the increasing angle of attack, as shown in Fig. 10. Similarly, the behavior is due to the relative reduction of the slope of the rear diagonal edge length.

In incompressible flow conditions relatively high thickness to chord ratios are acceptable and give a good structural depth with a small profile drag penalty. At higher Mach numbers, where compressibility effects become important, it is usual to use somewhat thinner airfoil (Howe & Rorie, 2000). When calculating the drag force in transonic or supersonic flow, the effects due to the formation of shock waves have to be considered. By examining the RS at the transonic regime, it was observed that by increasing the thickness, the drag coefficient increases intensity at 0° and 5° angle of attack, but this effect decreases with increasing angle of attack. The lift coefficient approximately is constant. Increased thickness means higher wave drag in transonic and supersonic flight regime (Roskam, 2002). In a supersonic flight regime, the wave drag is proportional to the parameter $(t/c)^2$, because of very rapid increase of wave drag with t/c , the thickness of wing must be selected very carefully (Roskam, 2002). This change in thickness has an

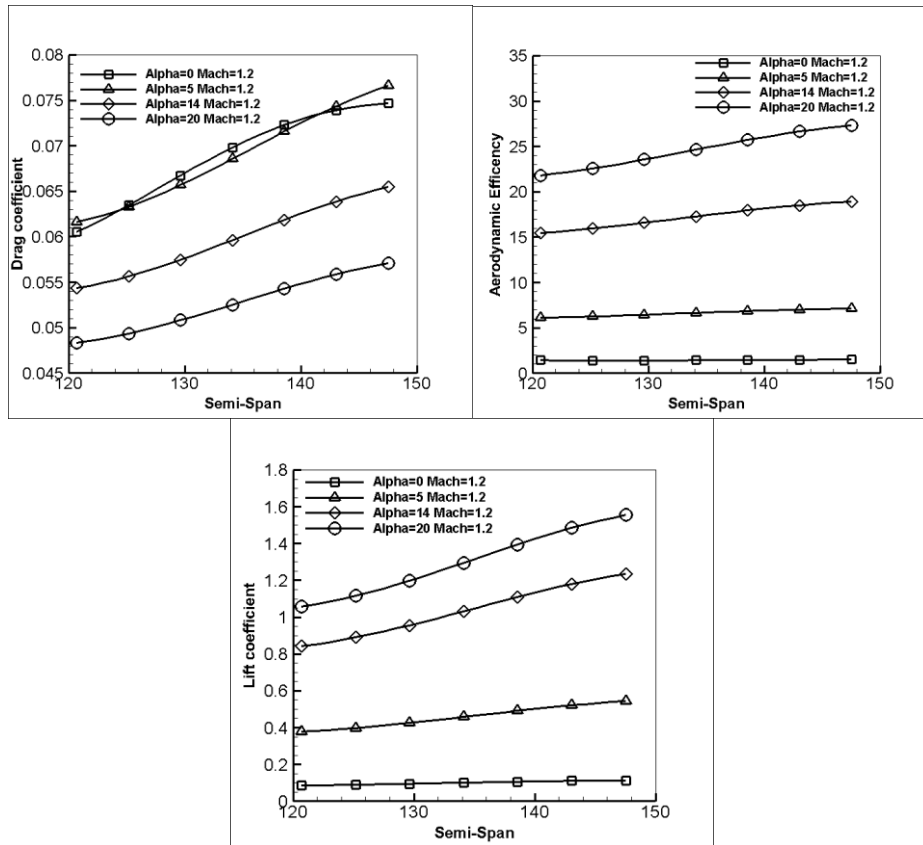


Fig. 13. Effect of increasing Span on the objective functions at $M=1.2$ and $AOA=0, 5, 14$ and 20° .

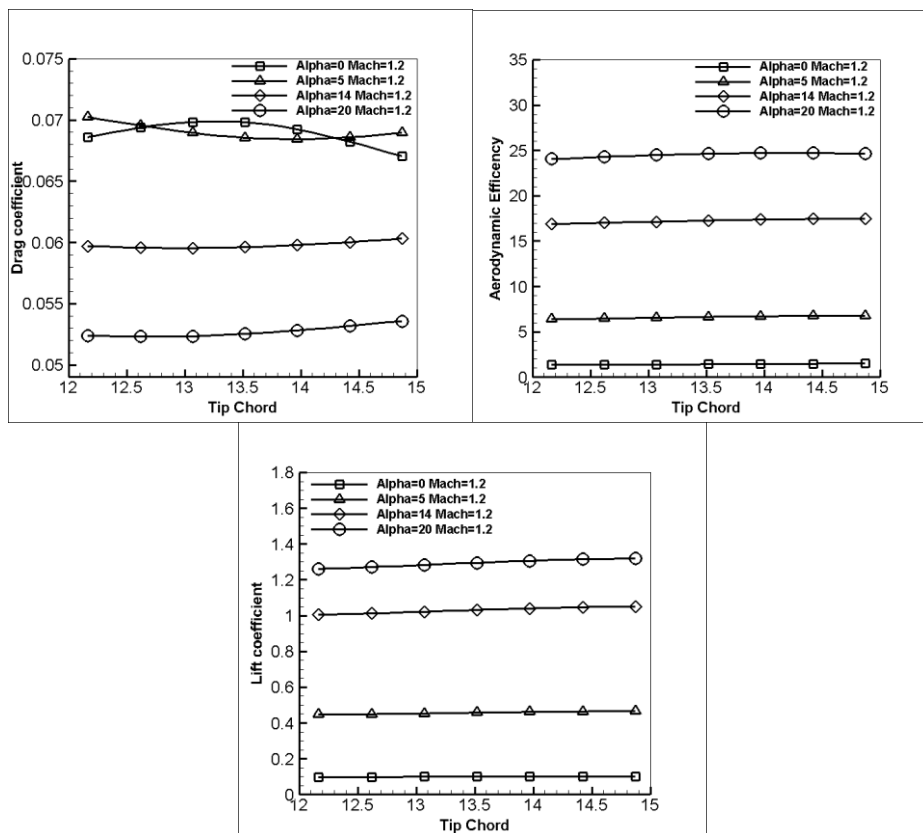


Fig. 14. Effect of increasing tip chord on the objective functions at $M=1.2$ and $AOA=0, 5, 14$ and 20° .

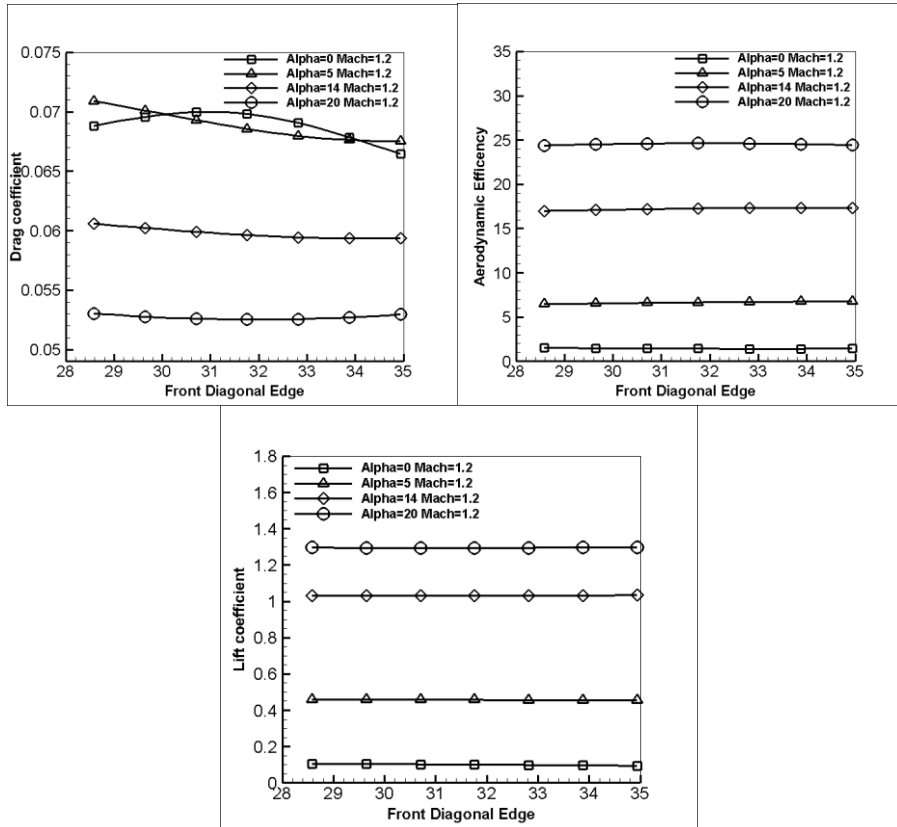


Fig. 15. Effect of increasing front diagonal edge length on the objective functions at $M=1.2$ and $AOA=0, 5, 14$ and 20° .

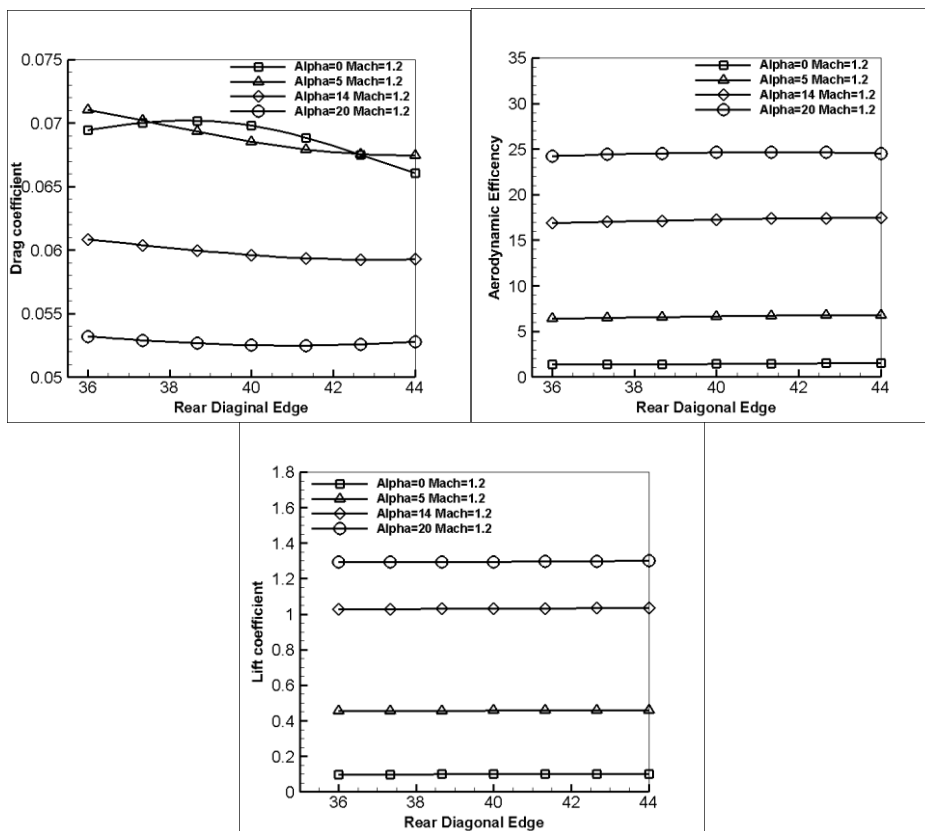


Fig. 16. Effect of increasing rear diagonal edge length on the objective functions at $M=1.2$ and $AOA=0, 5, 14$ and 20° .

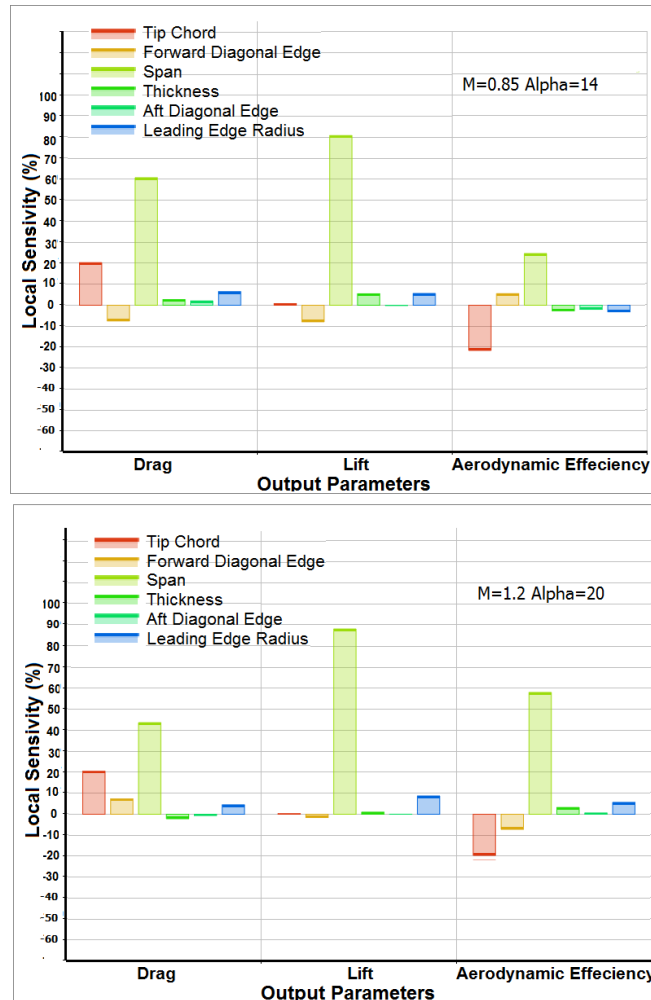


Fig. 17. Local sensitivity shows the weight of each parameter around the response point (Left side: M=0.85, Alfa=14 and Right side: M=1.2, Alfa=20).

insignificant effect on the aerodynamic performance shown in

Increasing the leading edge radius at M=1.2, increases the drag coefficient at all angles except the zero angle of attack, but does not affect the lift coefficient. The change in leading edge radius does not have much impact at low AOAs, but with the increase of the AOA, the aerodynamic efficiency decreases slightly. This process is presented in Fig. 12 Wing Span is one of the entrances that has a great impact on both the lift and drag forces and both of them increase at M=1.2. The effect of this increase on the lift coefficient is greater than the drag, which increases with increasing the AOA which is also observed in the aerodynamic efficiency of the wing. Fig. 13 shows this trend. The effects of increasing the wing size and aspect ratio ($AR=b^2/S$) due to the increasing span described earlier are also here.

Increasing the tip chord on the drag coefficient has a little incremental effect on this coefficient at transonic regime. But this behavior varies from zero angle of attack to others, so that it first increases and then decreases. Of course, the increase in the tip chord length always has a slightly positive effect on

the lift force, which increases with increasing the AOA. In total, the increase in the wing tip chord has improved the aerodynamic efficiency shown in Fig. 14. The effects of increasing the taper ratio ($TR=C_t/C_r$) due to the increasing tip chord described earlier are also here.

Table 4 Model Summary

Objective Functions	R	R Square	Adjusted R Square	Std. Error of the Estimate
Aerodynamic Efficiency	0.962	0.926	0.914	0.672
Drag Force	0.967	0.935	0.925	56.543
Lift Force	1.000	0.999	0.999	285.700

At the M=1.2, increasing the front and rear diagonal edge lengths in the lift and drag coefficients are the same and has little effect, except at the zero angle of attack, which reduces drag, is negligible in the rest of the cases. This behavior is due to pass off smoothly flow from the upper surface of wing. Also it is not

Table 5 ANOVA for Regression of RSM

Model		Sum of Squares	df	Mean Square	F	Sig.
Aerodynamic Efficiency	Regression	214.019	6	35.670	79.081	0.000
	Residual	17.140	38	.451		
	Total	231.159	44			
Drag Force	Regression	1745922.496	6	290987.083	91.015	0.000
	Residual	121491.171	38	3197.136		
	Total	1867413.666	44			
Lift Force	Regression	3545851182.799	6	590975197.133	7240.173	0.000
	Residual	3101729.313	38	81624.456		
	Total	3548952912.112	44			

Table 6 Candidate points characteristics

Candidate Point	M=0.85 Alpha=0	M=0.85 Alpha=5	M=0.85 Alpha=14	M=0.85 Alpha=20	M=1.2 Alpha=0	M=1.2 Alpha=5	M=1.2 Alpha=14	M=1.2 Alpha=20
Tip chord (cm)	14.86	12.36	14.20	13.65	14.84	14.69	14.65	14.152
Front Diagonal edge length (cm)	31.84	33.56	33.42	30.53	29.74	34.77	33.94	28.616
Half span (cm)	135.63	135.09	121.03	146.69	129.17	131.69	138.22	136.24
Thickness (cm)	7.41	7.34	8.76	8.92	7.33	7.32	7.35	7.31
Rear Diagonal Edge length (cm)	40.86	43.81	38.15	37.46	43.84	43.68	40.32	38.45
LE Radius (cm)	2.74	2.56	2.33	2.29	2.69	2.62	2.32	2.25
Drag (N)	846	689	199	371	2294	2492	2427	2106
Lift (N)	5042	11744	15513	26946	4174	19122	47528	56638
Aerodynamic Efficiency	5.73	16.70	66.08	65.42	1.80	7.62	19.53	26.83

affected on the lift coefficient. Altogether, this trend is reflected in the aerodynamic efficiency as shown in Local Sensitivity shows the norm of the partial derivatives of the chosen object with respect to the selected variables. The local sensitivity of each output parameter to the input parameters is illustrated in Fig. 17. which shows the weight of each input parameters around the response point. The two situations that are displayed are very important. The position of M=1.2 and AOA=20° is the situation of the highest angle of attack at the ascent trajectory, and M=0.85 and AOA=14° is the moment of 1st stage engine start up. It can be seen that in both situations, drag force and aerodynamic efficiency is most affected by span and tip cord.

An ANOVA (analysis of variance), which is one of the data mining techniques, is carried out to differentiate the contributions to the variance of the response surface from the model. To evaluate the effect of each design variable, the total variance of the model is decomposed into that of each design variable and their interactions. This method is used to identify unnecessary terms in model function has been considered. In Table 4 and Table 5 the model summary and ANOVA for Regression of RSM at Mach=1.2 and AOA=20° have been shown respectively. The mean difference is significant at the 0.05 level. According to the data of Table 5, the Adjusted R Square of the model for aerodynamic

efficiency is 0.926, so it can be concluded that 93% of the variation of the design variable can be attributed to changes in the objective function, and 7% of the changes due to other factors. The multiple regression coefficient is 0.962 which means that the severity of the relationship between the design variables and objective function is 96%. As shown in Table 5, sig. is zero and less than significance level (= 0.05), which indicates that at least one of the design variables has a linear relationship with the objective functions. The results of this analysis for lift and drag forces are similarly shown in the Table 4 and Table 5.

4.3 Optimization Study Results

The DoE table was populated with 46 DPs, hereinafter referred to as 46-DP, using a central composite design (CCD) method. The DoE table is first filled in by the sampling values in the design space. Each design parameter can be combined with others at different levels. The DoE table is generated using the optimization software DX (Design eXplorer) by ANSYS. The results (Adeeb, Sohn, Maqsood, & Afaq, 2018) confirmed the successful application and implementation of DOE and RSM to solve industrial problems related to product design and manufacturing. In Table 3, the initial design parameters, constraint values, and objective function values has been shown.

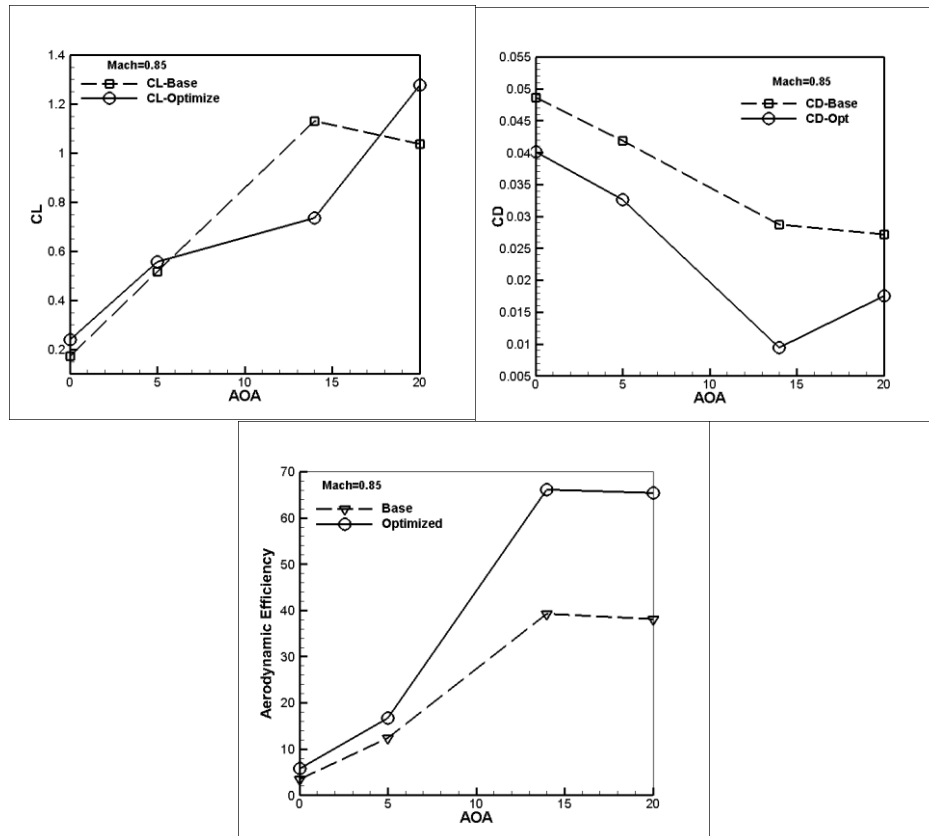


Fig. 18. Lift and Drag coefficients and aerodynamic efficiency of initial and optimized wing at different AOAs in Mach=0.85.

Multi-objective genetic algorithm (MOGA) as the numerical optimization technique and RSM, combined with the DOE have been used to optimize. The MOGA method used in this research is a hybrid variant of the NSGA-II (Non-dominated Sorted Genetic Algorithm-II) based on controlled elitism concepts. This method has simple handling of constraints and excellent multi-objective performances. It has good flexibility with regard to setting design constraints and objectives (Zhao, Zhang, Chen, Chen, & Zhang, 2016). The optimum points found by the optimizer for each flow regime are listed in Table 6. Analyzed regimes include Mach 0.85 and 1.2 at angle of attacks of 0, 5, 14, and 20 degrees. It can be seen that in both flow regimes, the best aerodynamic efficiency (L/D) is achieved at an angle of attack of 20 degrees. Therefore, the best point for optimizing the air-launching vehicle delta wing in the ascent trajectory is can be the maximum AOA that occurs in Mach 1.2. Accordingly, the Delta Wing is mounted on the model and is optimized in the conditions described above, which will be published in another article. In this optimization, the objective function was determined first. There are three objective functions considered in Multi-objective optimization algorithm. The objective functions are Drag force (to be minimized), Lift force (to be maximized) and the aerodynamic efficiency is the lift to drag ratio which has been maximized as an objective function. The optimizer was set to find three candidate points at each Mach number and

AOA, which were then verified. In Table 6, the candidate points features are illustrated.

The drag coefficient of a wing consist of the parasite drag due to airfoil (C_d), the induced drag due to production of the lift (C_{Di}) and the wave drag due to generation of shock waves. Parasite drag is independent of lift and increases with airspeed and depends on the airfoil shape, Reynolds number, AOA and surface roughness. Induced drag will be at its maximum when airspeed is low, thus with a large AOA. Induced drag grows with increasing of the angle of attack and decreases with increasing speed where parasite drag will increase to cumulatively form the total drag of a wing. The drag curve in ref (Anderson Jr, 2010) shows that total drag is high at slow (high AOA and mainly induced drag) and high airspeed (low AOA and mainly parasite drag). Minimum drag is experienced somewhere in the middle where the aerodynamic efficiency is at its highest. The variation of lift and drag coefficients and aerodynamic efficiency for different AOA's at both Mach numbers are shown in Fig. 18. and Fig. 19. At the transonic flight regime, due to the presence of shock, the amount of drag coefficients are higher than the high subsonic flight mode. Zero-lift drag is not only composed of a skin-friction drag but additionally consists of a wave (or pressure-related) drag at zero lift. Similarly, the lift-dependent drag is not only composed of induced drag but also of the drag due to lift (Dailey, 2005).

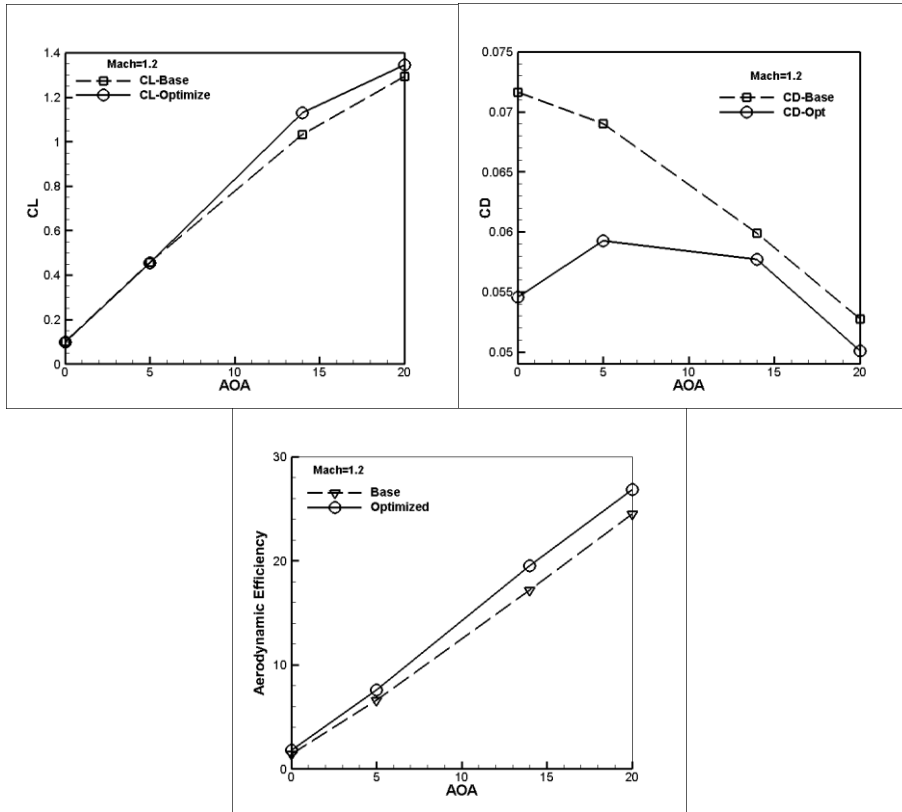


Fig. 19. Lift and Drag coefficients and aerodynamic efficiency of initial and optimized wing at different AOAs in Mach=1.2.

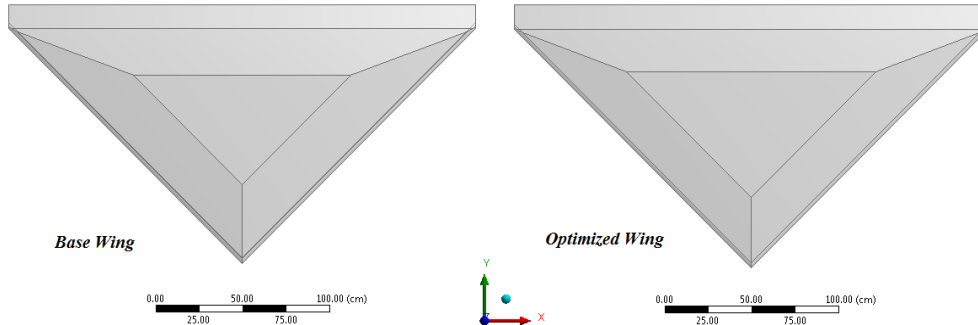


Fig. 20. Comparison of initial (left side) and optimized wing (right side) configurations.

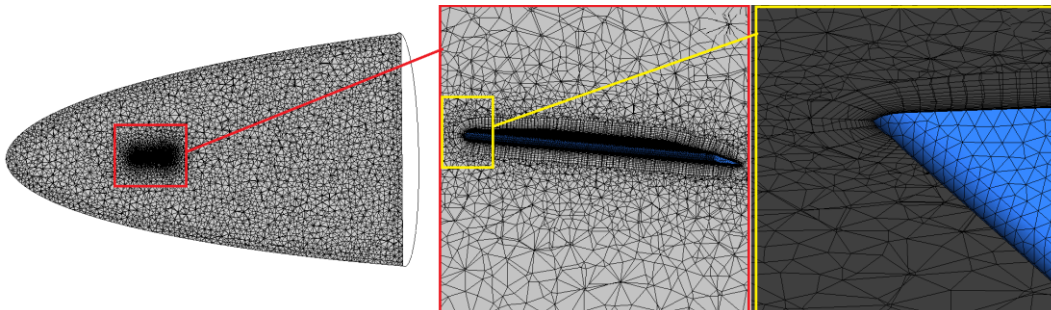


Fig. 21. CFD grids with 971,000 hybrid mesh.

This design involves many advantages including reduced drag and increased aerodynamic efficiency and is able to meet the mission requirements under

different flight conditions to ascent the LEO orbit. The results are given in Table 7 clearly show that optimization offers better performance than the

based model vehicle in terms of the drag force (increase 13.9%), lift force (increase 56.5%) and aerodynamic efficiency (increase 27.9%). Of course, shrinking the wing in optimization procedure of the air-launching vehicle based on the achievement of the required lift (which is less than half the production lift) and minimizing the drag, also reduces the weight of the rocket, which has a positive impact on overall performance. Also in Fig. 20. the initial and optimized wing configurations has been illustrated.

Table 7 Base and optimized designs comparison (M=1.2 and AOA=20 deg.)

Model	Lift (N)	Drag (N)	Aerodynamic Efficiency
Benchmark Design	41342	1848	22.4
Optimized layout	64728	2106	28.65
Relative difference (%)	56.5	13.9	27.9

In Table 8 the characteristics of the base wing and optimized values have been shown. It is observed that geometric modification which leads to optimized layout consist of increasing wing area by 3.7%, wing span by 1.6%, tip chord 4.6% and decreasing the thickness by 10% compared with benchmark design.

Table 8 basic and optimized values

Quantity	Basic	Optimal value	Relative difference (%)
Wing Area (cm ²)	21.6	22.42	3.7
wing span (cm)	268.24	272.48	1.6
Root Chord (cm)	147.6	150.4	1.9
Tip Chord (cm)	13.52	14.15	4.6
Thickness (cm)	8.12	7.31	10
Aspect Ratio	3.33	3.31	0.6

5. CONCLUSION

An excellent explanation of transonic flow phenomena is given by John D. Anderson. Transonic flow is one of the most challenging topics in aerodynamics. This paper has been focused on the evaluation of the effects of Non-slender delta wing design variables on the aerodynamic efficiency based on CFD and DOE via RSM in transonic flow regime. For this purpose, it has been considered a clipped delta planform with a modified double wedge airfoil section used for the air-launch-to-orbit vehicle (Aelaei, Ommi, & Karimian, 2017). The reason for delta wing selection, mainly is the lack of wind tunnel data for design process while it is flying in a wide range of Mach numbers. The Thickness, wing-span, tip chord, leading edge radius, frontal edge length and rear edge length are defined as

geometric design variables. The performance issues or the objective functions are minimizing the drag force, maximizing the lift force as well as aerodynamic efficiency. The pitching moment is important in the control and stability of the rocket, which is determined on the basis of such parameters as weight and initial launch conditions at the detailed design phase. Due to the configuration of the rocket, it is easy to change the location of the wing to achieve the required pitching moment, and the main moment generated by the lift force with the its arm, so in this simulation, in order to reduce the calculation, the pitching moment analysis are neglected.

The validation of the numerical method is satisfied by Pegasus rocket flight test data. The DOE table with 46 design points has been introduced versus 8 flight conditions. Using DX design space and solving the all design points by FLUENT, then it can be created the RS via ANSYS which appropriately describe the objectives in terms of parameters. Finally utilizing the NSGA-II method, the optimized solution has been proposed. With respect to available parallel processing system, the analysis has been carried out at Mach 0.85 and 1.2 and for AOA=0, 5, 14 and 20 degrees. A total of 368 cases (46 design points at 2 Mach numbers and 4 Angle of Attacks) were solved and evaluated. An analysis and implementation of the ANOVA for RSM have been performed and the results show that 93% of the variation of design variables can be attributed to changes in the objective functions. In this investigation it was observed that the wing span has the highest direct effect and the thickness has the most adverse effect on aerodynamic efficiency. In the optimized design, although increasing drag by 14% has been revealed, but the lift coefficient has been enhanced by 56.5% and therefore progress in aerodynamic efficiency (*L/D*) by 28% has been achieved compared with benchmark. By Examining the weight of each parameter around the response point, it can be seen that suitable critical design candidate point is combination of M=1.2 and AOA=20°. By guarantee for this point the minimum drag and the best aerodynamic efficiency in both flow regimes and different angle of attacks will be brought up. Therefore, the best point for optimizing the air-launched vehicle delta wing in the ascent trajectory is the maximum AOA that occurs in Mach 1.2.

REFERENCES

- Adeeb, E., E. Sohn, C. Maqsood and M. Afaq (2018). Design Optimization of Ceiling Fan Blades with Nonlinear Sweep Profile. *Journal of Applied Fluid Mechanics* 11(5).
- Aelaei, M., F. Ommi and S. Karimian (2017). Accuracy Evaluation of Semi-empirical and Numerical Methods in Estimation of Aerodynamic Coefficients for air-launch-to-orbit delta wing (in Persian). *Modares Mechanical Engineering* 17(9), 207-216.
- Anderson Jr, J. (2010). *Fundamentals of*

- aerodynamics*. Tata McGraw-Hill Education.
- Anderson, J. (2003). *Modern Compressible Flow with Historical Perspective*. New York: McGraw-Hill Companies.
- Bardina, J., P. Huang and T. Coakley (1997). Turbulence modeling validation. *28th AIAA Fluid Dynamics Conference, AIAA-1997-2121*.
- Barret, C. (1996). *Review of Our National Heritage of Launch Vehicles Using Aerodynamic Surfaces and Current Use of These by Other Nations: Center Director's Discretionary Fund Project Number 93-05*. National Aeronautics and Space Administration, Marshall Space Flight Center.
- Bertelrud, A., G. De la Tova, G. Budd, G. Noffz, W. Richards and R. Monaghan (2000). *Pegasus Wing-glove Experiment to Document Hypersonic Crossflow Transition: Measurement System and Selected Flight Results*. NASA, Dryden Flight Research Center.
- Bertin, J. and L. M. Smith (1998). *Aerodynamics for engineers*.
- Breitsamter, C. (2008). Unsteady flow phenomena associated with leading-edge vortices. *Progress in Aerospace Sciences* 44(1), 48-65.
- Dailey, J. (2005). *Centennial of Flight: Transonic Flow*.
- ANSYS *DesignXplorer User's Guide* (2016). Workbench.
- Elsayed, M., M. Scarano and N. Verhaagen (2008). Leading-Edge Shape Effect on the Flow over Non-Slender Delta Wings. *46th AIAA Aerospace Sciences Meeting and Exhibit* (p. 344).
- Engelund, W., D. Stanley, R. Lepsch, M. McMillin and R. Unal (1993). *Aerodynamic configuration design using response surface methodology analysis*. NASA STI/Recon Technical Report A, 94.
- Godil, A. and A. Bertelrud (1992). Design of a wing shape for study of hypersonic crossflow transition in flight. *Computing Systems in Engineering*, 3(1-4), 115-130.
- Görtz, S. (2005). *Realistic simulations of delta wing aerodynamics using novel CFD methods*. Doctoral dissertation, KTH.
- Gülsaçan, B., g. Şencan and M. Yavuz (2018). Effect of Thickness-to-Chord Ratio on Flow Structure of a Low Swept Delta Wing. *AIAA Journal*, 56(12), 4657-4668.
- Gursul, I. (2005). Review of unsteady vortex flows over slender delta wings. *Journal of Aircraft* 42(2), 299-319.
- Gursul, I., R. Gordnier and M. Visbal (2005). Unsteady aerodynamics of nonslender delta wings. *Progress in Aerospace Sciences* 41(7), 515-557.
- Gursul, I., W. Zhijin and V. Elen (2007). Review of flow control mechanisms of leading-edge vortices. *Progress in Aerospace Sciences* 43(7-8), 246-270.
- Howe, D. and G. Rorie (2000). *Aircraft conceptual design synthesis*. Professional Engineering.
- Hyun-Su, K. and K. Youn-Jea (2016). A Study on the Multi-Objective Optimization of Impeller for High-Power Centrifugal Compressor. 9(2), 143-149. *International Journal of Fluid Machinery and Systems* 9(2), 143-149.
- Jacob, M., W. Bret and H. Peter (2016). *Optimization of an Aircraft Wing*. MAE 598 – Design Optimization.
- Kleijnen, J. (2015). *Design and Analysis of Simulation Experiments*. Springer, 2nd edition.
- Lian, Y., S. Wei, V. Dragos and Z. Baoning (2003). Membrane wing aerodynamics for micro air vehicles. *Progress in Aerospace Sciences* 39(6-7), 425-465.
- Malik, M., L. Fei and C. Meela (2007). Analysis of Crossflow Transition Flight Experiment aboard the Pegasus Launch Vehicle. *AIAA paper 4487*.
- Manshadi, M. and M. Jamalinasab (2017). Optimizing a Two-Element Wing Model with Morphing Flap by Means of the Response Surface Method. *Iranian Journal of Science and Technology, Transactions of Mechanical Engineering* 41(4), 343-352.
- Mendenhall, C. (1983). *Delta Wings: Convair's High-speed Planes of the Fifties & Sixties*. Motorbooks International.
- Mendenhall, M. R. (1994). Aerodynamic design of Pegasus-Concept to flight with computational fluid dynamics. *Journal of Spacecraft and Rockets* 31(6), 1007-1015.
- Mitchell, J. and K. A. Ramesh (2016). *Computational Fluid Dynamics Simulation and Optimization of 69-Degree-Delta Wing Model in Supersonic Flow*. Washington University Open Scholarship, Mechanical Engineering and Materials Science Independent Study.
- Morton, S., J. Forsythe, A. Mitchell and D. Hajek (2002). DES and RANS simulations of delta wing vortical flows. *40th AIAA Aerospace Sciences Meeting & Exhibit*, (p. p. 587).
- Nangia, R. (2008). Semi-Empirical Prediction of Vortex Onset and Progression on 65 deg. Delta Wings (RTO-AVT-113, VFE-2 Facet). *46th AIAA Aerospace Sciences Meeting and Exhibit*.
- Noffz, G. K. (1991). *Noffz, Gregory K., et al. Aerothermal test results from the first flight of the Pegasus air-launched space booster*. NASA.
- Polhamus, E. (1968). *Application of the leading-edge-suction analogy of vortex lift to the drag due to lift of sharp-edge delta wings*.
- Ridolfi, L., M. Pontani and P. Teofilatto (2010).

- Effect of different flight conditions at the release of a small spacecraft from a high performance aircraft. *Acta Astronautica* 66(5), 665-673.
- Roos, F. and J. Kegelman (1990). An experimental investigation of sweep-angle influence on delta-wingflows. *28th Aerospace Sciences Meeting*, (p. 383).
- Roskam, J. (2002). *Airplane Design Part 3: Layout Design of Cockpit, Fuselage, Wing and Empennage: Cutaways and Inboard Profiles*. DARcorp, Lawrence, KS.
- Taylor. G., T. Schnorbus and I. Gursul (2003). An
- Verhaagen, N. and M. Elsayed (2008). Effects of Leading-Edge Shape on the Flow Over 50-deg Delta Wings. *26th AIAA Applied Aerodynamics Conference*, (p. p. 7330).
- Younis, Y., A. Bibi, A. Haque and S. Khushnood (2009). Vortical flow topology on windward and leeward side of delta wing at supersonic speeds. *Journal of applied fluid mechanics* 2(2), 13-21.
- Zhao, T., Y. Zhang, H. Chen, Y. Chen and M. Zhang (2016). Supercritical wing design based on airfoil optimization and 2.75 D transformation. *Aerospace Science and Technology* 56, 168-182.